17èmes JOURNEES DE L'HYDRODYNAMIQUE
JH2020

24 - 26 novembre 2020
CHERBOURG - en - COTENTIN

Marine growth effect on the hydrodynamical behavior of a submarine cable under current and wave conditions.

A. Marty[(1),*], C. Berhault[(2)], G. Damblans[(2)], J-V. Facq[(1)], B. Gaurier[(1)], G. Germain[(1)], T. Soulard[(3)], and F. Schoefs[(4)]

[(1)]Ifremer, Marine Structure Laboratory, 150 Quai Gambetta 62200 Boulogne sur Mer, France
[(2)]France Energies Marines, Brest, France
[(3)]Centrale Nantes, 1 rue de la Noë, 44321 Nantes, France
[(4)]Université de Nantes, 2 rue de la Houssinière, 44322 Nantes, France
[*]Corresponding author: antoine.marty@ifremer.fr

Résumé

Ce document décrit les essais réalisés dans le cadre des projets OMDYN2/LEHERO-MG ([1], [2]) au bassin d'essais de Boulogne sur mer. Le but de ces essais est de quantifier les effets du biofouling sur le comportement dynamique d'un câble électro-porteur à partir de l'analyse des coefficients hydrodynamiques de traînée et de masse ajoutée s'appliquant sur un cylindre circulaire colonisé ou non par des concrétions marines rigides de grandes dimensions de type moule. Le montage expérimental permet d'étudier le comportement de différents types de cylindres instrumentés : cylindre sans rugosité et cylindre comportant des macro rugosités. La fixation de la maquette sous un hexapode positionné à la verticale de la section d'essais permet de réaliser des essais en courant seul, en mouvements imposés et en mouvements imposés avec courant. Les coefficients obtenus, adimensionnalisés par le diamètre équivalent, montrent des résultats sensiblement identiques pour les essais en courant seul en présence ou non de macro-rugosités, mais diffèrent d'un facteur trois pour les cas en mouvements imposés et mouvements imposés avec courant.

Summary

This document describes the experimental set-up of OMDYN2 [1] and LEHERO-MG [2] projects. The study aims to quantify the impact of biofouling on the dynamic behaviour of an underwater power cable by analysing the hydrodynamic coefficients, such as drag and added mass coefficients. Experiments have been carried out in the wave and current basin of IFREMER, located at Boulogne-sur-mer, in order to compare the dynamics of several cylinders with or without roughness. Three cylinders are tested, two cylinders with different roughnesses and one smooth cylinder. The studied roughnesses concern realistic marine growth and have therefore significantly bigger dimensions (like mussels) than roughness studied in the research literature on the subject. Tests are conducted using current only then horizontal movements only and finally the combination of both. Results show that the calculated coefficients are notably similar when comparing cylinders in currents only but are very differents with the presence of motions. Indeed, drag coefficients can be three times higher for cylinders with roughness than without.

1. Introduction

Most of the Floating Wind Turbine sites are located in moderate water depths where biofouling can be observed on a major part of the water column with high roughness at high Reynolds Number. Damblans & Schoeffs [3] mentioned that applying the DNV rules (see API [4] and DNV [5] standards) on a 30 MW cable may multiplied the mass of the cable by a factor of 2 in water, so impacting drastically the static lazy/steep-wave layouts with possible contact with seabed. These recommended practices involve an added mass increase by a factor greater than 5 so impacting the hydro-mechanical dynamics and reducing the fatigue life. Because biofouling is space, time and material dependent, general empirical certifications widely used in the engeenir-ing field which take into account the biofouling influence in the design process are limited due to the small number of rugosity already studied. Indeed, the flow around objects with circular cross section has received considerable attention, motivated by the fundamental flow phenomena involved as well as for its relevance to engineering applications, such as mooring lines or power cables. One of the general characteristic features is the appearance of fluctuating hydrodynamic loads which can lead to flow-induced vibrations and, if low damped, to possible structure damage. The possible influences of rough surfaces on the flow phenomena and on the surface pressures and forces acting on a circular cylinder have been investigated in many aspects already but most often with relative low roughnesses.
This is the reason why we performed a dedicated basin test campaign under the OMDYN 2 project (partners: France Energies Marines, Bureau Veritas, RTE, Naval Energies, ENSTA, EDF, Univ. Nantes, Centrale Nantes, Atlantique Offshore Energy, Ifremer, Total, Innosea). These tests are carried-out at full-scale, so removing the Reynolds similitude issue, with a highly realistic representation of mussel's colonization through 3D printing covers, defined by statistical analysis of in-situ observations at SEMREV-test site [6]. Then, accurate description of inertial impacts (mass and radiated field) are provided as well as the viscous effect in reproducing close fluid shearing due to surface irregularities, often called "roughness". In this study, the cable is represented by a 160 mm diameter rigid tube with or without 3D printing roughness with external diameter up to 280 mm.
After a quick description of the process used to experimentaly simulate mussels concretion on a cable, we propose to present the results of the experimental campaign carried out in the wave and current circulating tank of Ifremer [7]. The mean drag coefficient and the vortex shedding frequency for trials under current and the added mass coefficient for the trials under combined current and forced motions will be compared for three configurations.

2. Experimental set-up

Tests are carried out in the wave and current circulating flume tank of IFREMER located in Boulogne-sur-Mer (France). The incoming flow is assumed to be steady and constant inside the test section of 18 m long $\times$ 4 m wide $\times$ 2 m deep. By means of a grid combined with a honeycomb (that acts as a flow straightener) placed at the inlet of the working section, a low turbulent intensity of $I = 1.5$ % is achieved. In this work, the three instantaneous velocity components are denoted (U,V,W) along the (x,y,z) directions respectively. Using the Reynolds decomposition, each instantaneous velocity component is separated into a mean value and a fluctuation part: $U(X,t) = \overline{U(X)} + u'(X,t)$, where an overbar indicates the time average.

2.1 Assembly and instrumentation

An overview of the global set-up is presented on figure 1. The cylinder movements are generated using a 6-axis hexapod on which the structure and the intrumentation are installed. As shown on the figure 1, the cylinder is horizontally mounted so that the cylinder is located in the middle of the test section (at one meter depth). The cylinder is perpendicular to the direction of the upstream flow. The axis coordinate system (x, y, z) is choosen so that the Ox axis is in the same direction than current. The Oz axis is across the width of the basin and the Oy axis is vertical and oriented upwards, see figure 2.
Two 6 components loads cells, with a maximal loads range of $F_{x,y,z} = 150$ daN (measurement accuracy

0.75 N), fixed at each extremity of the cylinder allow a measurement of the forces applied on the cylinder. The location of these loads cells is identified by their own axis system as shown on the figure 2. The two cylindrical loads cells measure the forces applied on the cylinder only, half of the total load for each cell.

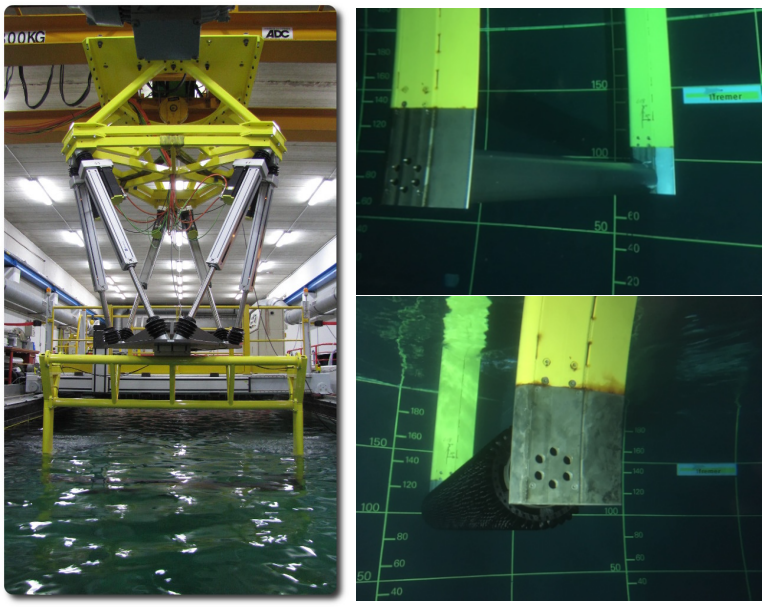

Figure 1. Presentation of the global set-up with the smooth cylinder (top right) and the rough cylinder (bottom right).

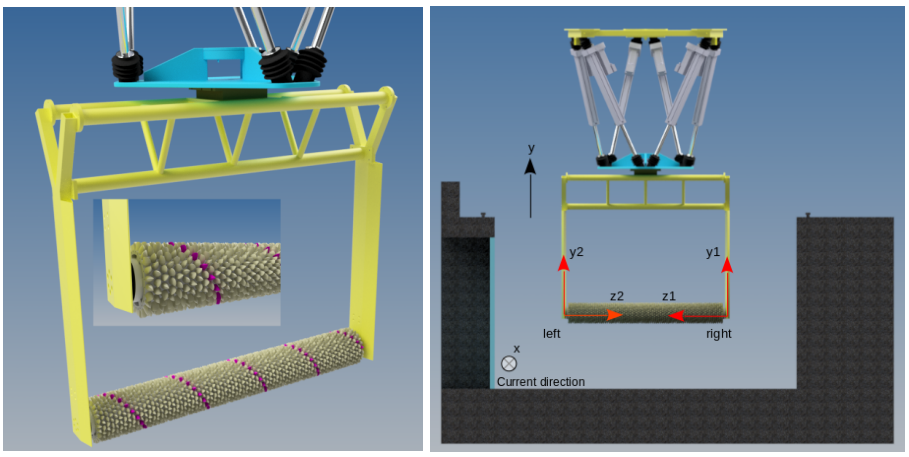

Figure 2. Axis coordinate system (x, y, z) used in tests. In black, the main system. The Ox axis is common to all systems and corresponds to the main flow direction. In red, the axes of the loads cells (right and left).

2.2 Diameters and roughness definition

The experimental set-up is based on a smooth cylinder (S , $D_i = D_{ext} = D_e = 160\,mm$) on which the roughness is superimposed in order to design a configuration with roughness, see Figure 3. To this end, two types of mussel distributions have been considered. The first one called $C1$ with outside diameter equal to 260 mm with small size mussels and the second one called $C2$ with outside diameter equal to 280 mm composed of larger individual mussels. The charasteristics of the studied configurations are listed on table 1.
The roughness parameter is defined as the ratio k/D_e, where k is the dimension of the studied roughness and D_e the equivalent diameter. In the literature, several definitions of the roughness exist, see Achenbach and Heinecke (1981) [8]. In [9], Ameryoun et al. used a stochastic modeling of marine growth and hydrodynamic parameters to define the roughness as the ratio of the apparent height of the surface roughness (mussel length from the wider section to the external extremity) on the equivalent diameter of the studied configuration. A mussel cover may be composed of several highly compact superimposed layers. As such, layers below the

external one represent a thickness of closed surfaces where no fluid dynamics is permitted, with no entrapped water volume. Consequently, this thickness is assumed to be a diameter increase in a fluid dynamic point of view. Then, the thickness is defined only from the external layer. Applying the same principle on the external layer, the part below the wider section of the mussel is considered closed. Consequently, only the mussel height upon the wider section is considered to define the roughness k, representing the surface irregularities impacting the flow boundary layer. Figure 3 represents the different parameters for the calculation of the roughness for each kind of mussels ($C1$ and $C2$). The equivalent diameter is calculated as follow: $D_e = D_i + 2 \times (S - k)$.

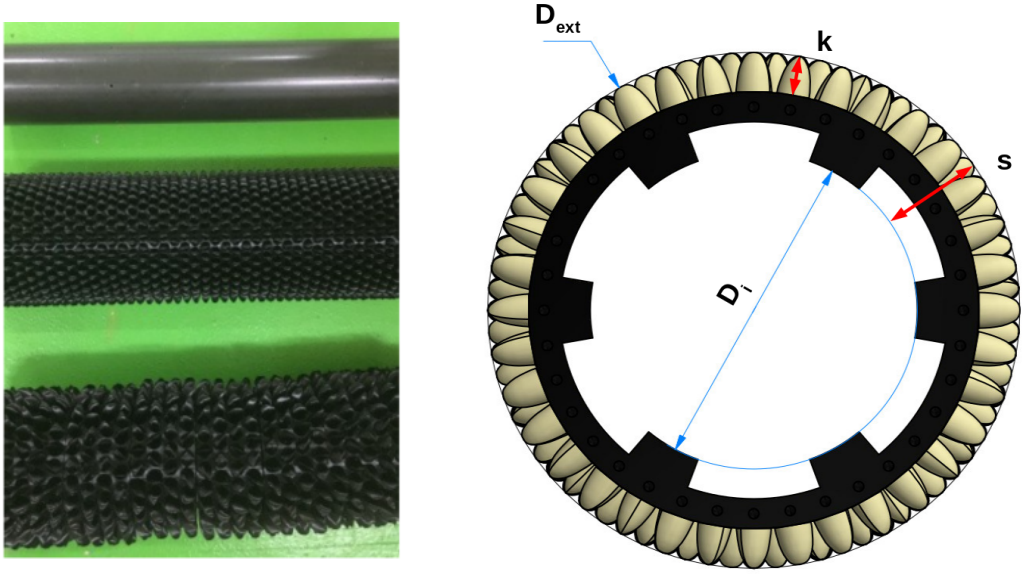

Figure 3. Illustration of the three studied configurations (left) and definition of the roughness parameters (right)

Configuration	S	C1	C2
D_i (mm)	160	160	160
S (mm)	0	50	60
k (mm)	0	20	30
D_{ext} (mm)	160	260	280
D_e (mm)	160	220	220
$R_{ec} = k/D_e$	0	0.091	0.136
Mass system (daN)	47	105	110

Table 1. Synthesis of the studied configuration parameters of the three cases

2.3 Test cases

Table 2 summarizes the main test conditions which has been imposed to the tested configurations. Tests have been carried out in current only first, then in oscillating movements without current and in a third time the combination of both.

	Current Alone	Motion Alone	Current + Motion
U $(m.s^{-1})$	0.25 - 1.5	-	0.25 - 1.5
Amplitude A_x (mm)	-	100 - 400	100 - 400
Frequency f (Hz)	-	0.1 - 0.75	0.1 - 0.75

Table 2. Flow and motion parameters for the three configurations with A_x and f the motion amplitude and frequency.

All the results are presented as a function of the classical normalized numbers which are defined as follow:

- Reynolds number (R_e) defined in two different ways depending on the choice of the reference speed, the flow velocity U or the oscillation speed $A_x\,\omega$:

$$R_e = \frac{UD_e}{\nu} \quad \text{or} \quad Re = \frac{A_x\,\omega D_e}{\nu}, \text{ with } \nu \text{ the kinematic viscosity.}$$

- Keulegan-Carpenter number (K_c) defined by the equation :

$$K_C = 2\pi\frac{A_x}{D_e} \tag{1}$$

- The reduced speed (U_r) for current and movements cases :

$$U_r = \frac{U}{fD_e} \quad \text{with} \quad f = \frac{\omega}{2\pi} \tag{2}$$

The table 3 summarizes the value ranges of the three normalized numbers used in this study.

Configuration	S	C1	C2
K_c	3.9 - 15.7	2.8 - 11.4	2.8 - 11.4
U_r	4.1 - 39.1	3 - 56.8	3 - 56.8
$Re/10^5$	0.4 - 2.7	0.55 - 3.3	0.55 - 3.3

Table 3. Synthesis of the normalized numbers of the three cases

2.4 Calculation method of hydrodynamic coefficient

In current only, the drag coefficient is calculated as follow:

$$C_D = \frac{2 \times \overline{F_D(t)}}{\rho S U^2} \tag{3}$$

with ρ the density of water ($\rho = 998\ kg/m^3$), $S = D_e \times L$ the cylinder section in front of the flow and U the current velocity. $\overline{F_D(t)}$ is the temporal mean of the drag $F_D(t)$. This coefficient is also called *steady-flow drag coefficient*.
In the case of oscillating motions, the hexapod moves along the Ox axis, colinear with the current. The hexapod movements are oscillating with an amplitude A_x and a pulse $\omega = 2\pi f$ such as: $x(t) = A_x\cos(\omega t + \varphi_x)$. It is assumed that the answer of this excitation is a sinusoidal function as well (it is also assumed that the harmonics higher than 1 are neglected). Thus, the drag effort may be expressed as follows.

$$F_D(t) = F_m\cos(\omega t + \varphi_F) \tag{4}$$

Hence, with $\varphi = \varphi_F - \varphi_x$ it comes :

$$F_D(t) = -\frac{F_m\cos(\varphi)}{A_x\,\omega^2}\,\ddot{x}(t) + \frac{F_m\sin(\varphi)}{A_x\,\omega}\,\dot{x}(t) \tag{5}$$

This equation 5 can be compared with the Morison's equation [10] :

$$F_D(t) = -\rho C_m L\frac{\pi {D_e}^2}{4}\,\ddot{x}(t) + \frac{1}{2}\rho C_d D_e L\,\dot{x}(t)\,|\dot{x}(t)| \tag{6}$$

with C_m the inertia coefficient ($C_m = (C_a + 1)$, with C_a the added mass coefficient) and C_d the drag coefficient. Moreover, $\sin\omega t\,|\sin\omega t|$ can be approximated with $\sin\omega t$, and more precisely with :

$$\sin\omega t\,|\sin\omega t| \simeq \frac{8}{3\pi}\sin\omega t \tag{7}$$

And finally, by comparison:

$$\begin{cases} C_m = \dfrac{F_m \cos(\varphi)}{\rho L \frac{\pi D_e^2}{4} A_x \omega^2} \\ C_d = \dfrac{F_m \sin(\varphi)}{\frac{4}{3\pi} \rho D_e L A_x^2 \omega^2} \end{cases} \tag{8}$$

These coefficients are the same as the standard API [4] and are called *Inertia and Drag Coefficients*.
For current and motions cases it is assumed that the drag effort can be divided into two parts, the mean drag part $\overline{F_D(t)}$ and the oscillating part $F_m \cos(\omega t + \varphi_F)$, such as:

$$F_D(t) = \overline{F_D(t)} + F_m \cos(\omega t + \varphi_F) \tag{9}$$

Thus, the three coefficients C_D, C_m ans C_d can be calculated similarly as previous (equations 3 and 8). These three parameters are plotted as a function of the dimensionless numbers previously cited (R_e, K_c and U_r). All the raw data can be found on the data share platform SEANOE, see [11].

3. Roughness effect on cylinder loads

3.1 Current only test

Figure 4 shows the evolution of the drag forces in function of the flow velocity. In the studied flow range, there is no drag force differences between the two roughness. The curves highlight the classical evolution according to a square power law for the two rough cylinders. This response is however different for the smooth cylinder with a linear evolution until the transition obtained at a flow speed of $1.25 m/s$. For $U > 1.25 m.s^{-1}$, the drag is quite constant around $F_D \approx 200N$.

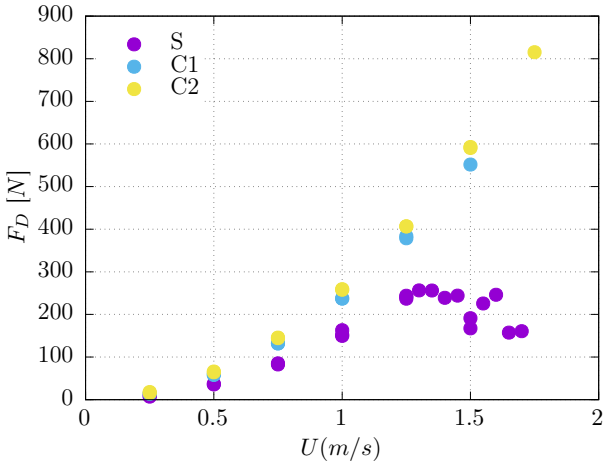

Figure 4. Drag force evolution for the three tested cases

The variation of the overall mean drag coefficient C_D, the Strouhal number $S_t = \frac{f_v L}{U}$ (with f_v the vortex shedding frequency) and the r.m.s. values of the lift with Reynolds number are presented in figure 5. For the smooth case, the overall shape of the $C_D(Re)$ curve clearly coincides with the results presented in the litterature. In the subcritical Reynolds number regime a nearly constant value for C_D of about 0.9 is found. For increasing Reynolds numbers, hence by approaching the critical flow state or lower transition that starts at $R_e \approx 2.1.10^5$, this value gradually decreases. The minimum value of the drag coefficient of $C_D \approx 0.28$ at $R_e \approx 2.10^5$ marks the transition from the critical Reynolds number regime to the upper transition. This phenomenom is well known [12], [13] and confirms the accuracy of the experimental set-up and of the measurements. For roughness cases ($C1$ and $C2$) the transition does not occur in the flow velocity range studied. The results show that

C_D increases with the size of the roughness, reaching a nearly constant value of about 1.05 for C_1 and 1.15 for C_2.
Figure 5 presents the dependency of the Strouhal number, $S_t = \frac{f \times D_e}{U}$, on the Reynolds number. A constant value of $S_t = 0.18$ is observed in the subcritical regime for the smooth cylinder. This value is lower than the Strouhal number commonly used which is generally equal to 0.21, see [14]. For both rough cylinders, the Strouhal number presents a nearly constant value of about 0.14.
The variation of the r.m.s values of the lift fluctuations with the Reynolds number is also shown in figure 5. A maximum value of approximately 0.3 is obtained for $R_e \approx 2.10^5$ in the subcritical state. For larger Reynolds numbers inside this flow regime a steep decrease of the r.m.s. values is observed. For both rough cases, the fluctuations are very low with: $C_l' \ll 0.05$.

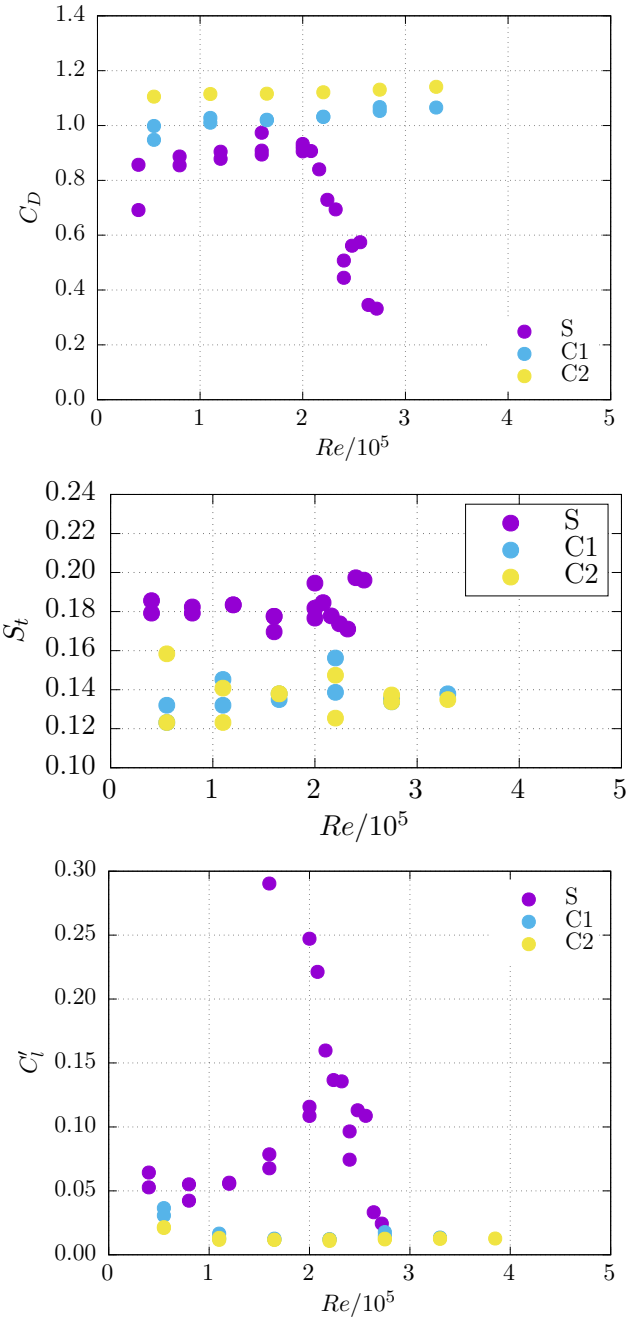

Figure 5. Distribution of the three main hydrodynamic parameters as function of the Reynolds number from direct force measurements for the three test cases: S, $C1$ and $C2$.

These results show that the surface roughness has an influence on the drag coefficient, the r.m.s. values of the lift fluctuations and the Strouhal number. The r.m.s. values are always lower for the rough circular cylinders. A

similar trend is observed on the drag coefficient, where a difference of about 10% between cases is observed in this range ($R_e < 2.10^5$). The vortices are shed into the wake with different frequencies. The Fourier transform of the lift forces shows (figure 6) that the amplitude peaks of the vortex shedding frequencies are much more higher for the smooth configuration with values of 25 N for $2 \leq R_e/10^5 \leq 2.5$ when it reaches only 2 N for the two rough configurations.

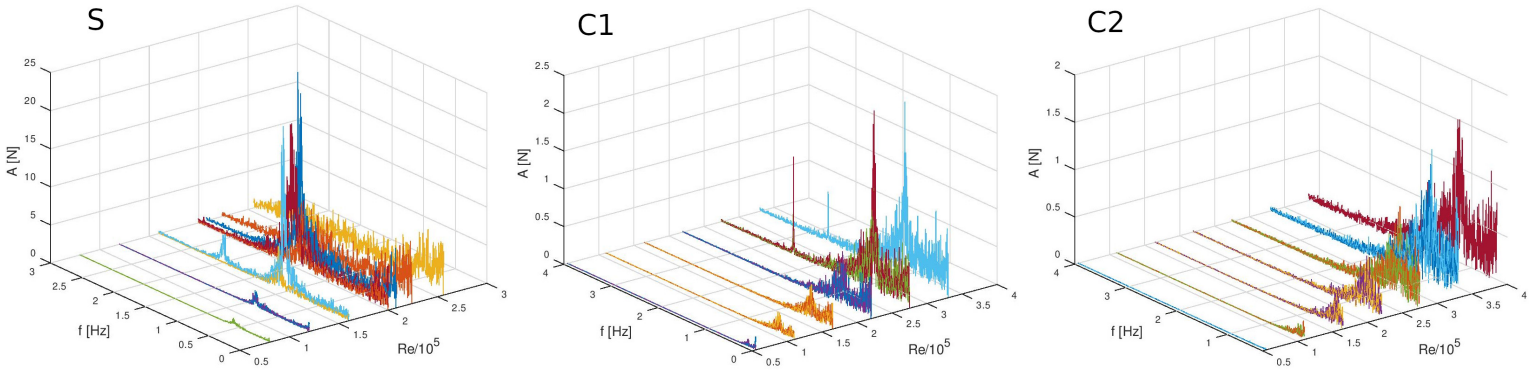

Figure 6. Lift forces Fourier transform as function of the Reynolds number for the three test cases: S, $C1$ and $C2$.

3.2 Oscillating motions

For the oscillating motions test cases, the current velocity is equal to zero. Figure 7 presents the evolution of the oscillating drag coefficient C_d (left) and the inertia coefficient C_m as a fonction of the Keulegan-Carpenter number K_c. Several points are plotted per K_c because several tests have been carried out at the same motion amplitude A_x but with different frequencies.

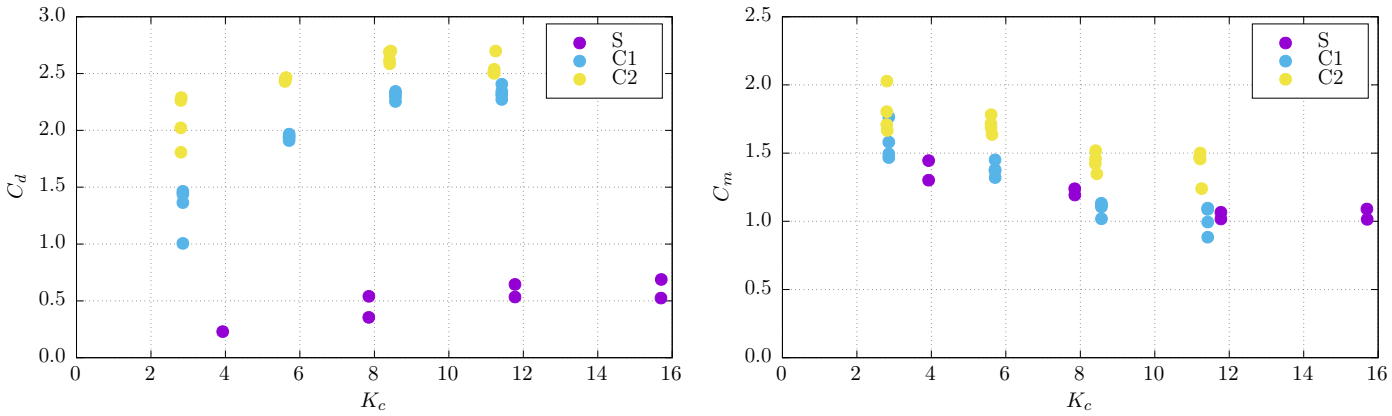

Figure 7. C_d (left) and C_m (right) vs K_c.

The results show that there is no significant difference between inertia coefficient even if the C_m of the smooth cylinder is slightly lower than the roughness cases, see figure 7 (right), and globally the behaviour for the two rough cylinders is quite the same in oscillating motions, C_2 is just slightly higher. However, there is an important difference concerning oscillating drag coefficients between smooth and rough cases. The calculated coefficients are more than three times higher for cases $C1$ and $C2$ compared to the smooth case, with $C_d \approx 2.5$ for $K_c > 6$ for the rough cases and $C_d \approx 0.5$ for $K_c \leq 16$ for the smooth cylinder. The behaviour of the rough cylinders is mainly governed by the flow and not by their motions, contrary to the smooth cylinder for which its behaviour is mainly governed by its motions.

3.3 Current and oscillating motions

This section presents results concerning current and oscillating motions tested cases. The same coefficients previously shown are calculated, which are the mean drag coefficient C_D, the oscillating drag coefficient C_d

and the inertia coefficient C_m. These coefficients are at first presented configuration by configuration as a function of U_r on figure 8. From these results, we can see that the coefficients for both roughness cases are not significantly different, particularly for the mean and oscillating drag which are very close. The inertia coefficients for the rough cases present less dispersion than for the smooth cylinder. For $U_r < 10$, the mean drag coefficients are two times higher for the rough cases than for the smooth one. These results confirm that the behaviour of the rough cylinders is mainly governed by the flow and not by their motions, contrary to the smooth cylinder for which its behaviour is mainly governed by its motions.
The figure 9 presents each coefficient for the three studied configurations. In order to compare the behavior of each configuration, the current velocity is fixed at 1 $m.s^{-1}$. These coefficients are represented as a function of the reduced speed for all the motion amplitudes in order to study the amplitude and the frequency parameters effects at the same time.
The results show several and opposite behaviours of the coefficients. First of all, the inertia coefficient (C_m) tends to be similar for each configuration. The higher the frequency (small U_r), the lower the coefficient. Moreover, we can conclude that the motion amplitude has no impact on the evolution of the inertia coefficient. Regarding drag coefficients (C_d and C_D), their behaviours are totally the opposite. The value of the coefficient C_d increases with the reduced velocity U_r. Moreover, for a fixed frequency (or U_r fixed) the amplitude parameter has a big impact and the value of the coefficient increases when the amplitude A_m decreases. The exact opposite phenomenom occurs concerning the mean drag coefficient C_D, with the value of the coefficient decreases when the amplitude A_m increases.
Finally, as for the previous case, there is an important difference concerning oscillating drag coefficients and mean drag coefficient between smooth and rough cylinders. The calculated coefficients are much more higher for cases $C1$ and $C2$ compared to the smooth case for wich there is no dependency on the motion amplitude and frequency. A strong dependency on the amplitude of the drag coefficients at fixed frequency for the rough cases is here clearly highlighted.

4. Conclusion and Perspectives

This study shows the impact of two realistics hard marine growth roughnesses on the drag and inertia coefficients compared to a smooth case. These results show that the surface roughness has an influence on the drag coefficient, the r.m.s. values of the lift fluctuations and the Strouhal number. The results from this experimental campaign do not highlight significant differences concerning the behaviour of the two rough cylinders ($C1$ and $C2$). The vortices are shed into the wake with different frequencies. The vortices are shed into the wake with different frequencies and different amplitudes, the amplitude peaks of the vortex shedding frequencies are much more higher for the smooth configuration than the rough configuration with a difference of about 90%. The r.m.s. values are always lower for the rough circular cylinders. A difference of about 10% between cases on the drag coefficient is observed for $R_e < 2.10^5$. For the oscillating cases, the inertia coefficients for the rough cases present less dispersion than for the smooth cylinder. For $U_r < 10$, the mean drag coefficients are two times higher for the rough cases than for the smooth one. In this case, a strong dependency on the amplitude of the drag coefficients at fixed frequency for the rough cases has been highlighted, while they are stable in static. This shows that the commonly used approach of $C_d = \psi(K_c).C_D(Re)$ is not legitimate. Moreover, while Morison's linearization for static drag force is justified, it means that it is not for oscillating cases, the KC defined only with the amplitude is not representative of the flow variety, this number should also depend on the frequency. These results highlight the fact that the behaviour of the rough cylinders is mainly governed by the flow and not by their motions, contrary to the smooth cylinder for which its behaviour is mainly governed by its motions.
For now, assumptions are strong: the marine growth is considered to be a homogeneous circumferential and length volume. Due to internal and inter-species competition, it has been observed that mussels are often arranged in a bulbous manner. This phenomenon has not been studied here but the roughness variations must be studied to be compared to homogenous cover which is considered in the engineering design phase. Pure current, regular forced oscillations and superimposed loadings must be tested in order to conclude on the validity

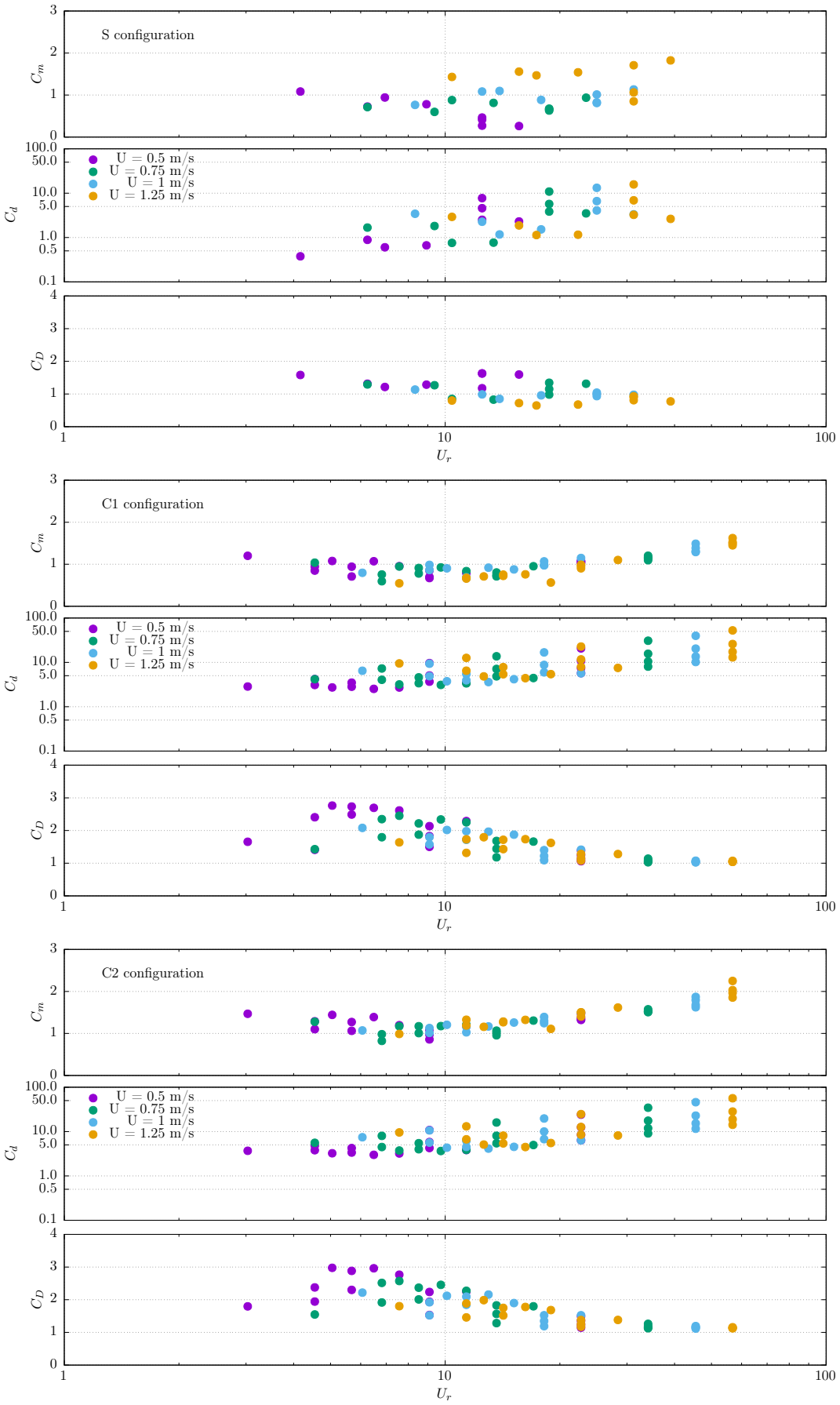

Figure 8. C_m, C_d and C_D vs K_c for the S (top), $C1$ (middle) and $C2$ (bottom) cases.

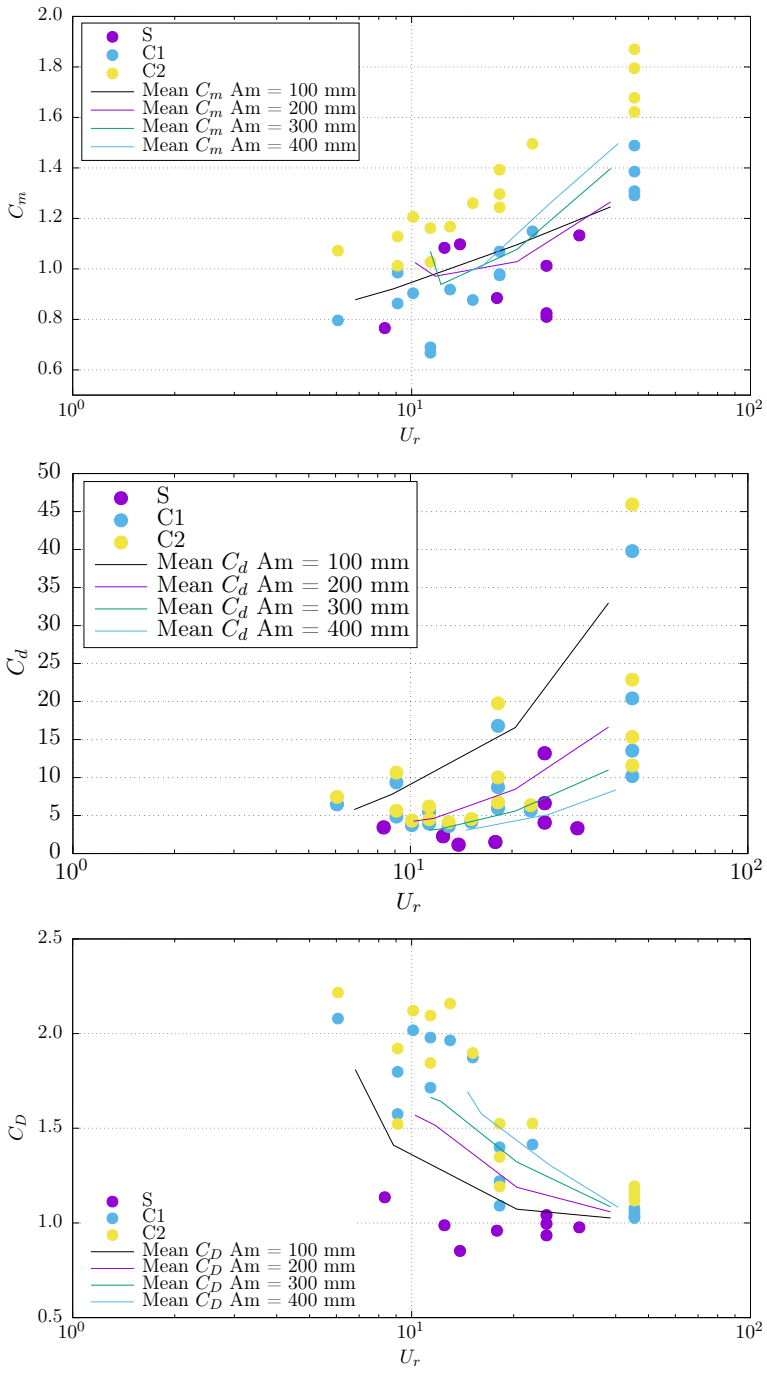

Figure 9. C_m, C_d and C_D vs U_r for the S, $C1$ and $C2$ cases.

of extracted coefficients but also on the standard hydrodynamic loading's formulation commonly used.

Acknowledgment

This work benefits from a French State grant managed by the National Research Agency under the Investments for the Future program bearing the reference ANR-10-IEED-0006-28. This project was partly financially supported by the European Union (FEDER), the French government, IFREMER and the region Hauts-de-France in the framework of the project CPER 2015-2020 MARCO. We are most grateful to Thomas Bacchetti for his participation conducting all the test campaign corresponding to about 800 cases.

References

[1] OMDYN2 - ANR - 10 - IEED - 0006 - 28, "https://www.france-energies-marines.org/r-d/,"

[2] LE HERO MG - WEAMEC, "https://www.weamec.fr/projets/lehero-mg/,"

[3] G. Damblans and F. Schoeffs, "Taking into account marine growth both at design steps and during exploitation," *FOWT*, 2017.

[4] American Petroleum Institute (API), "Planning, Designing and Constructing Fixed Offshore Platforms - Working Stress Design," API Recommended Practice 2A-WSD (RP 2A-WSD) twenty-first edition, American Petroleum Institute (API), Dec. 2000.

[5] DNVGL-OS-E301, "https://rules.dnvgl.com/docs/pdf/dnvgl/os/2015-07/dnvgl-os-e301.pdf,"

[6] B. Decurey, F. Schoefs, A. L. Barillé, and T. Soulard, "Model of bio-colonisation on mooring lines: Updating strategy based on a static qualifying sea state for floating wind turbines.," *J. Mar. Sci. Eng.*, vol. 8, no. 108, 2020.

[7] B. Gaurier, G. Germain, J. Facq, L. Baudet, M. Birades, and F. Schoefs, "Marine growth effects on the hydrodynamical behaviour of circular structures," *Proceedings of the 14th Journées de l'Hydrodynamique, Val de Reuil, France*, 2014.

[8] E. Achenbach and E. Heinecke, "On vortex shedding from smooth and rough cylinders in the range of Reynolds numbers 6e3 to 5e6," *Journal of fluid mechanics*, vol. 109, pp. 239–251, 1981.

[9] H. Ameryoun, F. Schoefs, L. Barrillé, and Y. Thomas, "Stochastic modeling of forces on Jacket-Type offshore structures colonized by marine growth," *Journal of Marine Science and Engineering*, vol. 158, May 2019.

[10] J. R. Morison, M. P. O'Brien, J. W. Johnson, and S. A. Schaaf, "The forces exerted by surface waves on piles," *Journal of Petroleum Technology*, vol. 2, pp. 149–154, May 1950.

[11] A. Marty, G. Germain, J. V. Facq, B. Gaurier, and T. Bacchetti, *Experimental investigation of the marine growth effect on the hydrodynamical behavior of a submarine cable under current and wave conditions*. IFREMER https://doi.org/10.17882/75373: SEANOE, 2020.

[12] R. L. P. Verley, *Oscillations of cylinders in waves and currents*. PhD thesis, Loughborough University of Technology, May 1980.

[13] H. Schlichting, *Boundary layer theory*. New York: McGraw-Hill book compagy, 1979.

[14] W. H. Melbourne and H. M. Blackburn, "The effect of free-stream turbulence on sectional lift forces on a circular cylinder.," *J. Fluid. Mech.*, vol. 11, pp. 267–292, 1996.